# Comparison of the Optical Lock-in Thermography using the Reflection Mode and the Transmission Mode

*Ondrej* Stalmach[1][0000-0003-3495-0330], *Vladimir* Dekys[1][0000-0001-5683-2058], *Vaclav* Straka[2], and *Katarina* Stalmachova[3]

[1]University of Zilina, Faculty of Mechanical Engineering, Univerzitna 1, 01026 Zilina, Slovakia
[2]TMV SS spol. s r. o., Studankova 395, 14000, Praha, Czech Republic
[3]University of Zilina, Faculty of Operation and Economics of Transport and Communications, Univerzitna 1, 01026 Zilina, Slovakia

**Abstract.** Optical lock-in thermography is a non-destructive testing method. The surface of the sample is excited using the thermal waves and the response is recorded by the thermal camera. This image thermal sequence is processed using the image processing method named lock-in method. Optical lock-in thermography can be used to detect cracks and damages in metal or composite material. Two position modes are used: the reflection and the transmission mode. In this paper, are compared these two modes. An experiment is carried out on a printed composite plane with the square blinded holes placed in the different depths below the surface. The phase images are created using the lock-in method for both position modes. The results are compared and the advantages and the disadvantage of these position modes find out.

## 1 Introduction

Over the last 20 years, thermography has been divided into active and passive thermography. At present, scientists are mainly focusing on the development of new methods in the field of active thermography. Active thermography differs from passive thermography in that the measured object must be excited by external source, e.g. using heat wave. Subsequently, the response is recorded using a thermal camera. Active thermography includes non-destructive testing (NDT) using thermographic systems [1-4], thermoelastic stress analysis [5-9], methods for assessing the fatigue of materials [10-16] etc.
The bestknown methods in the field of active thermography include:

- thermoelastic stress analysis (TSA),
- pulse thermography,
- pulse phase thermography,
- lock-in thermography,

- vibrotermography,
- rapid method for determining the fatigue limit.

## 2 Lock-in thermography

In the case of modulated heating of the body surface with a frequency *f*, a damped and scattered heat wave propagates in the subsurface region. In the plane layers of the body, it is possible to use the relation to evaluate the temperature *T* at the depth *z* and at time *t* [17]:

$$T(z,t) = T_0.e^{-\frac{z}{\mu}}.cos\left(\frac{2.\pi.z}{\lambda} - 2.\pi.f.t\right) \quad (1)$$

where $\mu$ is the depth of penetration of the heat wave at which the temperature drops to $\frac{1}{e^{T_0}}$, where $T_0$is the surface temperature of the body. The equation for $\mu$ is as follows [17]:

$$\mu = \sqrt{\frac{\kappa}{\pi.f.\varrho.c_p}} \quad (2)$$

$\kappa$ – thermal conductivity [W. m$^{-1}$. K$^{-1}$],
$\varrho$ – density [kg·m$^{-3}$],
$c_p$ – specific heat [J·kg$^{-1}$·K$^{-1}$],
$\lambda$ – thermal wavelength [m],
z – depth under the measured surface [m],
$f$ – frequency [Hz].

Lock-in thermography is based on heat waves generated inside the measured object by periodic (sine) excitation signal. The periodic excitation signal has a frequency called the lock-in frequency $f_L$. The heat wave (usually sinusoidal) penetrates the measured object and at the anomaly in the structure of the body is reflected to the surface. Interference of radiated and incident infrared radiation occurs on the surface of the object. As a result, the scanned thermograms are modified by a returning heat wave from inside of the measured object. In the lock-in thermography the frequency $f$ is changed to lock-in frequency$f_L$. A response is obtained for the selected $f_L$from a depth $\mu$below the surface of the measured object. In this way, it is theoretically possible to obtain a response over the entire material thickness range using different values of $f_L$.

The main idea of the lock-in thermography is the assumption that when the excitation signal has a sinusoidal character with frequency $f_L$, the recorded response will also have a sinusoidal character with the same frequency. It follows that the equation of the response can be written in the form:

$$s(t) = A.\sin(2.\pi.f_L.t + \varphi) = A.\cos\varphi\,.sin(2.\pi.f_L.t) + A.\sin\varphi\,.cos(2.\pi.f_L.t) = a.\cos(2.\pi.f_L.t) + b.\sin(2.\pi.f_L.t) \quad (3)$$

It is assumed that the amplitude $A$ of a given function $s(t)$can be very small and the measured signal $S(t)$ contains many times higher noise $N(t)$, according to the relation:

$$S(t) = s(t) + N(t) \quad (4)$$

If $S(t)$ is subsequently expressed by a Fourier series, where the noise $N(t)$is the term in square brackets:

$$S(t) = \frac{A_0}{2} + \sum_{i=1}^{\infty} A_i.(2.\pi.f_L + \varphi_i) = A_1.(2.\pi.f_L + \varphi_1) + \left[\frac{A_0}{2} + \sum_{i=2}^{\infty} A_i.(2.\pi.f_L + \varphi_i)\right] = a.\cos(2.\pi.f_L.t) + b.\sin(2.\pi.f_L.t) + N(t) \quad (5)$$

Then for $a, b, A_1, \varphi_1$are equations as follow:

$$a = A_1.sin(\varphi_1) \quad (6)$$

$$b = A_1.cos(\varphi_1) \quad (7)$$

$$A = A_1 \quad (8)$$

$$\varphi = \varphi_1 \quad (9)$$

The estimation of the parameters $a, b$ is determined by the estimates $a_{cos}, b_{sin}$using the relations of the discrete Fourier transform as follows:

$$a_{cos} = \sum_{i=1}^{N} S_i.cos(2.\pi.f_L.t_i) \quad (10)$$

$$b_{sin} = \sum_{i=1}^{N} S_i.sin(2.\pi.f_L.t_i) \quad (11)$$

$N$ – number of images in the recording from the thermal camera,
$S_i$ – $i$-th frames from a series of $N$ frames,
$t_i$ – time when the $i$-th image was taken.
Subsequently, for the phase of the harmonic function s$(t)$ is the equation as follow:

$$\varphi = atan\frac{a_{cos}}{b_{sin}} \quad (12)$$

## 3 Experimental measurement

Experimental measurement was performed in cooperation with the company TMVSS s.r.o. with office in Prague. The company lent the OTvis optical excitation system, the necessary InfraTecImageIR thermal camera and the premises in its building for the given experimental measurement.

### 3.1.Composite samples made on a 3D printer

Before the measurement, it was necessary to design and made test specimens. Two variants of test specimens - plates with dimensions 120 x 120 x 5 mm were proposed. The samples were made using a Mark TWO 3D printer and were made of Onyx material. No reinforcing fibers were used. The first variant contained 9 defects with a square cross-section with sides 10 x 10 mm (see Fig. 1). Defects were designed as blind holes of varying depth(from 0.5 to 4.5 mm, with 0.5 mm increments).

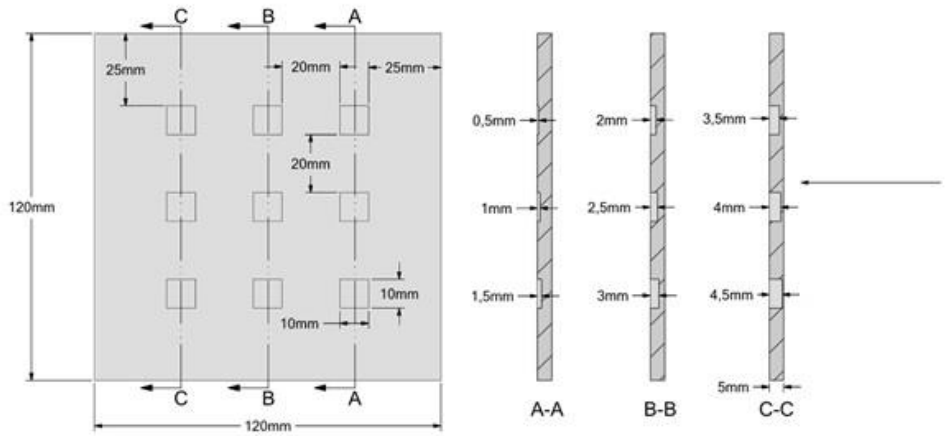


**Fig. 1.** Variant 1: dimensions of the sample with blind holes.

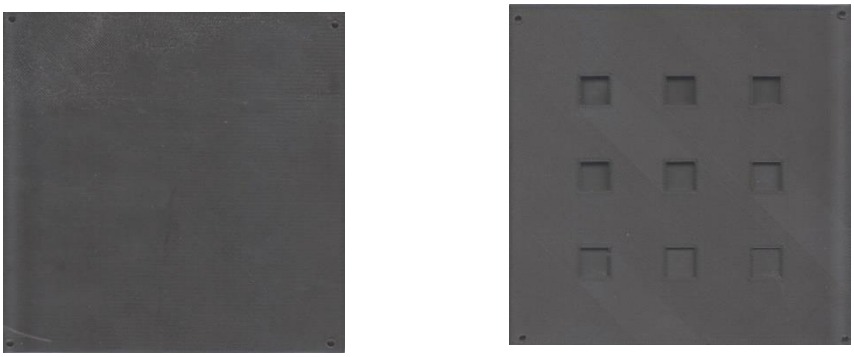

**Fig. 2.** Test plate variant 1: front / measuring surface (left) and back surface (right).

The second variant contained 9 block-shaped defects with dimensions 10 x 10 x 0.5 mm, spaced 20 mm apart. These were distributed at different depths below the surface (from 0.5 mm to 4.5 mm with 0.5 mm increments) (see Fig. 3).

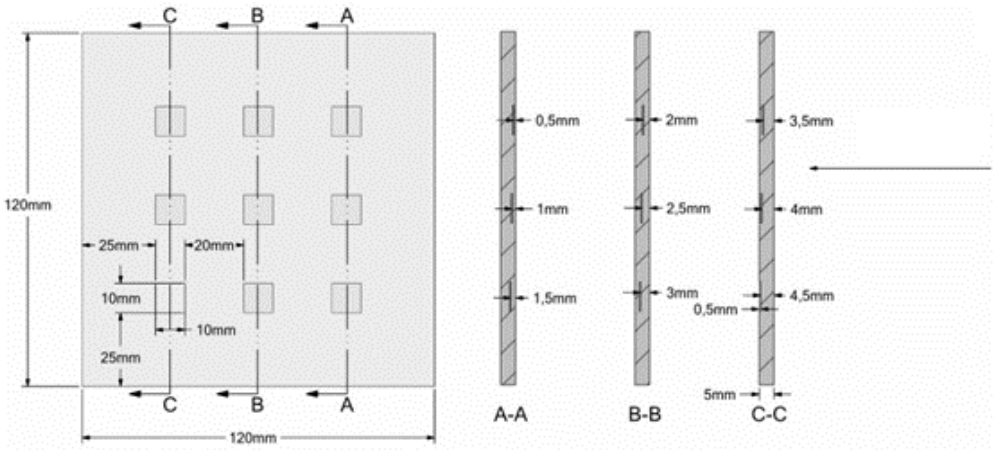


**Fig. 3.** Variant 2: sample dimensions.

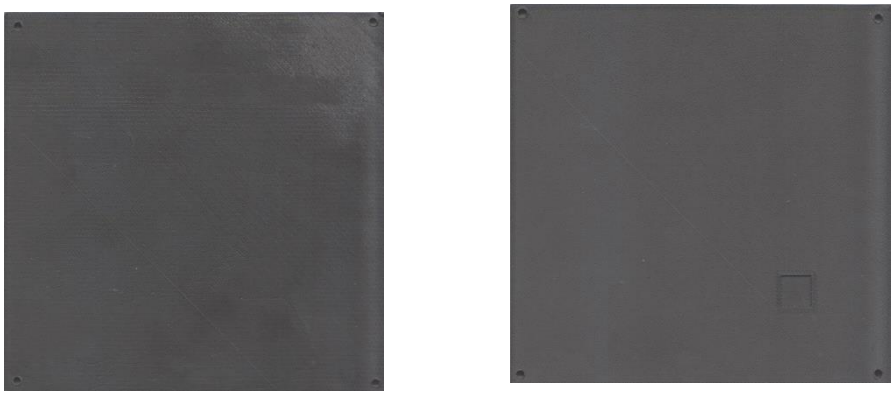

**Fig. 4.** Test plate variant 2: front / measuring surface (left) and back surface (right).

### 3.2.Settings of experiment measurement

Test samples were measured using optical lock-in thermography. A halogen lamp with the power 2.5 kW was used as the excitation source. An InfraTecImageIR thermal camera with a resolution of 640 x 480 pixels was used to record the response. The DisplayIMG software was used to process the measured data and evaluate the phase images.
Ten records were measured for the reflection method and 10 records for the transmission method, for both test samples. Ten records were made with different lock-in frequencies in order to obtain a response at ten different locations below the surface. Lock-in frequencies were calculated using the appropriate material properties as follows:

$$f_L = \frac{\kappa}{\pi.\varrho.c_p.\mu^2} = \frac{\alpha}{\pi.\mu^2} \quad (13)$$

Since the thermal conductivity $\kappa$ and the specific heat $c_p$ are not defined by the manufacturer of the Onyx material, their values could be expressed approximately (because the percentage of the individual components was known) using a mixing rule. Onyx is composed of 93% nylon and 7% carbon and therefore $\kappa$ and $c_p$ could be calculated as follows:

$$c_{p-onyx} = 0{,}93.c_{p-nylon} + 0{,}07.c_{p-uhlík} = 0{,}93.1510 + 0{,}07.717 = 1454{,}5\, J.kg^{-1}.K^{-1} \quad (14)$$

$$\kappa_{onyx} = 0{,}93.\kappa_{nylon} + 0{,}07.\kappa_{uhlík} = 0{,}93.0{,}23 + 0{,}07.1{,}7 = 0{,}33\, W.m^{-1}.K^{-1} \quad (15)$$

In the Table 1, the lock-in frequencies $f_L$ are calculated for the specified depths $\mu$ below the surface.

**Table 1.** Lock-in frequencies calculated for the specified depths below the surface.

| | 1. | 2. | 3. | 4. | 5. | 6. | 7. | 8. | 9. | 10. |
|---|---|---|---|---|---|---|---|---|---|---|
| $\mu$[mm] | 0.25 | 0.5 | 0.75 | 1.0 | 1.25 | 1.5 | 1.75 | 2.0 | 2.25 | 2.5 |
| $f_L$ [Hz] | 0.968 | 0.242 | 0.108 | 0.06 | 0.039 | 0.027 | 0.02 | 0.015 | 0.012 | 0.01 |

During the measurement, the test plate was attached to a polystyrene plate 1000 x 1000 x 50 mm, on which a black emission spray was applied. A hole 100 x 100 mm was made in

the middle of polystyrene plate. The test sample was attached so that there was a 20 mm overlap with the polystyrene plate on each side of the sample. Emission spray was applied to ensure more suitable surface properties of white polystyrene (reduction of reflectivity). The aim of this solution was to homogenize the environment around the test plate.
The thermal camera and the halogen lamp were placed at a distance of 1 m from the measured sample at an angle of approximately 40°. The lamp power was set to 50% of the power and the recording length was set to 4 excitation periods.

### 3.3 Reflection method

The reflection method consists in that the thermal camera and the excitation source (halogen lamp) are placed next to each other and the measured object is placed opposite (see Fig. 5).

**Fig. 5.** Reflection method.

The figure Fig. 6 and Fig. 7 shows the phase images for the individual responses from a depth $\mu$ below the measuring surface. Both variants of the test specimens were designed so that the first defect (defect in the lower left corner) was located 0.5 mm below the surface and each additional defect was placed 0.5 mm lower.
Material properties involved in the calculation of lock-in frequencies (thermal conductivity $\kappa$ and specific heat $c_p$ of Onyx) were only approximately calculated (equations (14) and (15)) and such a distribution of defects made it possible to verify their correctness. If the values of $\kappa$ and $c_p$ were calculated correctly, the corresponding defects should be displayed at 2. ($\mu$ = 0.5 mm), 4. ($\mu$ = 1 mm), 6. ($\mu$ = 1.5 mm), 8. ($\mu$ = 2 mm), 10. ($\mu$ = 2.5 mm), phase image (see Fig. 6 and Fig. 7).

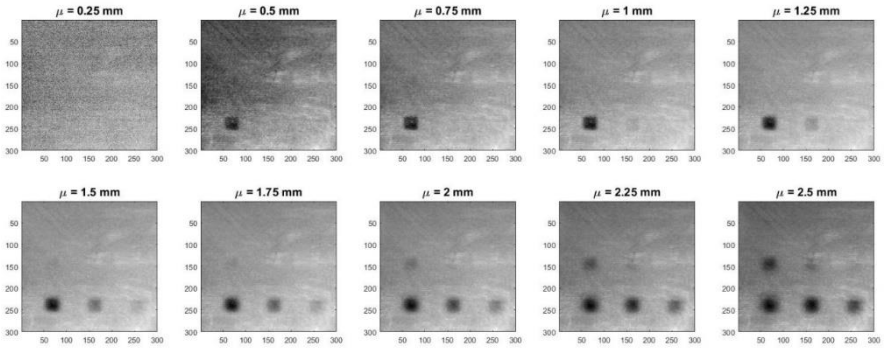


**Fig. 6.** Reflection method: phase images, variant 1.

In the figures of Fig. 6 and Fig. 7 it can be seen that the first defect (in the lower left corner) is displayed at a depth of $\mu$ = 0.5 mm and the second defect is slightly displayed at $\mu$ = 1 mm. The third defect is displayed at depth$\mu$ = 1.5 mm. The fourth defect is slightly displayed already at a depth of $\mu$ = 1.75 mm. The fifth defect is only minimally displayed at a depth of $\mu$ = 2.5 mm.
From a given measurement, it could be assumed that the calculated material properties of the values of $\kappa$ and $c_p$ were calculated correctly using the mixing rule (14) and (15).

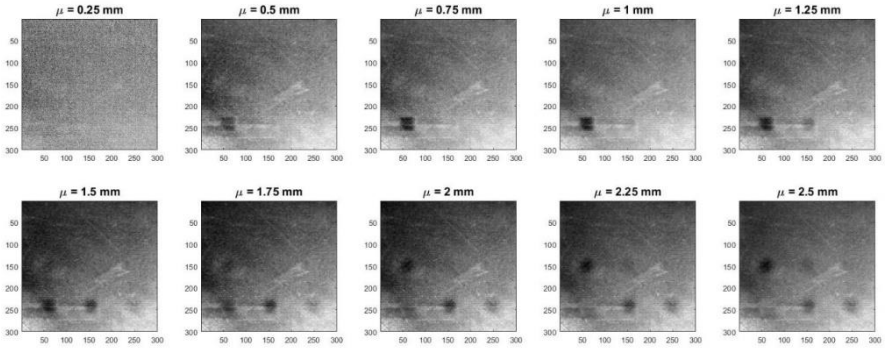


**Fig. 7.** Reflection method: phase images, variant 2.

### 3.4 Transmission method

The transmission method differs from the reflection method in that the measured object is placed between the thermal camera and the source of excitation. The thermal camera records the front / measuring surface of the object and the excitation source excites its back side (see Fig. 8).

The thermal camera was placed as in the reflection method and the halogen lamp was placed 1 m from the back surface of the polystyrene plate. The power setting of 50% and the recording length of 4 periods remained unchanged.

The figures Fig. 9 and Fig. 10 shows the phase images for both samples. It can be seen how the results for the reflection and transmission methods differ significantly. It can be seen from the measured data that it is possible to detect defects before they should be displayed according to heat wave theory. From the phase images, it can be observed that all

nine defects can be detected. The quality of the phase image display gradually increases up to a depth of μ = 1.5 mm. Subsequently, the image quality decreases and at a depth of μ = 2.25 mm, the phase image is damaged due to the saturation of the thermal camera detector.

**Fig. 8.** Transmission method.

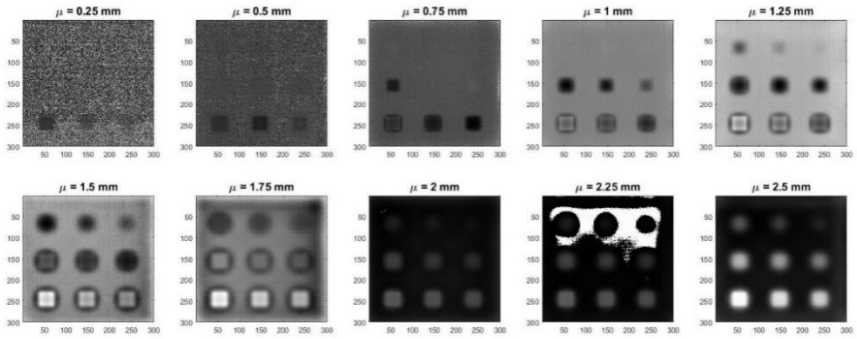


**Fig. 9.** Transmission method: phase images, variant 1.

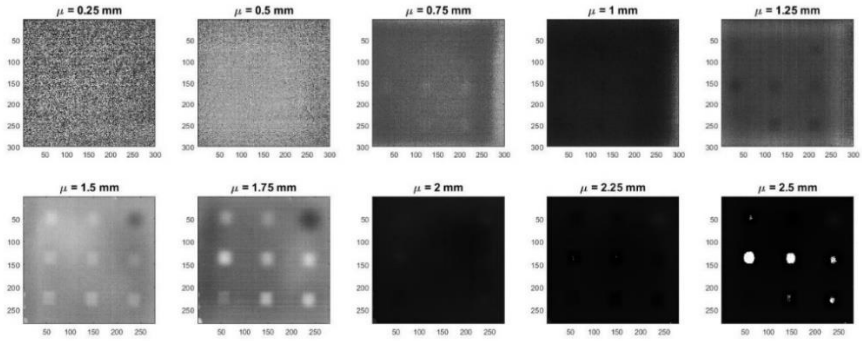


**Fig. 10.** Transmission method: phase images, variant 2.

## 4 Conclusion

From the measured data it can be seen that each of the methods (reflection and transmission) has its advantages and disadvantages. The advantage of the reflection method is that it is governed by heat wave theory. For this reason, it makes it possible to obtain information about the presence of a defect in the measured object and especially at what depth it is located below the surface. In this way, it was possible to gradually determine the depth at which the individual defects are located. On the other hand, the disadvantage is that the depth from which the response can be obtained is approximately 2.5 mm for the Onyx composite material. Due to this limitation, only five of the nine defects in the test plate could be detected. Also, the disadvantage is that the phase image obtained from a greater depth below the surface has a deteriorated imaging quality of the actual shape of the defects.

The transmission method isn´t follow the standard rules of heat wave theory, because defects were displayed earlier than they should have been. Therefore, it was not possible to obtain a response from a specific depth below the surface of the measured object (it was not possible to define at what depth below the surface the defects are located). However, the advantage over the reflection method is that with both variants of the test plates it was possible to detect all nine defects, which is also the main goal of the lock-in thermography.

The transmission method has a higher ability to detect the presence of defects (qualitative evaluation), while the reflection method provides good information on the morphology / shape and position of the defects (quantitative evaluation).

Another goal of the paper was to verify whether the values of the material parameters $\kappa$ and $c_p$ were calculated correctly using the mixing rule (14) (15). From the results of measurements using the reflection method we can observe that defects are displayed at lock-in frequencies at which they should be displayed according to the theory of heat wave. Therefore, we can consider the material parameters $\kappa$ and $c_p$ calculated using the mixing rule are correct.

### Acknowledgment

This work was supported by a grant agency VEGA 1/0141/20, VEGA 1/0510/20 and VEGA 1/0073/19.

### References

1. Z. Stankovicova et al. Nondestructive testing of metal parts by using infrared camera STFT. Procedia Engineering, 177, 562-567 (2017).
2. A detection of deformation mechanisms using infrared thermography and acoustic emission. Applied Mechanics and Materials, 474, 315-320 (2014).
3. L. Jakubovicova et al. Experimental and computational comparative study of the specimens loaded by bending and torsion. MATEC Web of Conferencesvol 157 (2018).
4. M. Sapieta et al. Using of active thermography and lock-in method with ultrasound exication for detection of material defects. Scientific Journal of Silesian University of Technology - Series Transport, 84, 119-124 (2014).
5. M. Sapieta et al. Comparison of the thermoelastic phenomenon expressions in strainless steels during cyclic loading. Metalurgija, 56, 203-206 (2017).
6. M. Sapieta et al. Thermal-stress analysis of beam loaded by 3 point bending. Procedia Engineering, 136, 216-219 (2016).
7. A. Sapietova et al. Dynamic and Stress Analysis of a Locking Mechanism in the Ansys

Workbench Software Environment. Advances In Science And Technology-Research Journal, 13, 23-28 (2019).
8. Z. Stankovicova et al2016 Time average synchronization in thermoelastic stress analysis. Procedia Engineering, 136, 204-210 (2016).
9. M. Honner et al. Survey of emissivity measurement by radiometric methods. Applied Optics, 54, 669-683 (2016).
10. Z. Stankovicova et al. Fatigue limit estimation using IR camera. MATEC Web of Conferences, 157 (2018).
11. V. Dekys et al. Simplified estimate of fatigue damage based on dynamic analysis. Scientific Journal of Silesian University of Technology-Series Transport, 99, 15-23 (2018).
12. P. Kopas et al. Low-cycle fatigue behaviour of laser welded high-strength steel DOMEX 700 MC. MATEC Web of Conferences, 157 (2018).
13. M. Saga et al. Contribution to fatigue damage prediction of thin shell finite element models. MATEC Web of Conferences, 157, (2018).
14. M. Saga et al. Modeling and Experimental Analysis of the Aluminium Alloy Fatigue Damage in the case of Bending - Torsion Loading. Procedia Engineering, 48, 599-606 (2012).
15. Sapieta M et al2018 Monitoring the fatigue crack on the test specimen during the cyclic loading(MATEC Web of Conferences vol157)
16. M. Sapieta et al. Determine the fatigue life of flange of bearings test station. Procedia Engineering, 177, 548-553 (2017).
17. M. Kreidl et al. Technická diagnostika. BEN - Technická Literatúra vol 1. (2006).